Endoscopic Add-on Stiffness Probe for Real-time Soft Surface Characterisation in MIS

A. Faragasso, A. Stilli, J. Bimbo, Y. Noh, H. Liu, T. Nanayakkara, *Member, IEEE*, P. Dasgupta
H.A. Wurdemann, K. Althoefer, *Member, IEEE*

***Abstract*— This paper explores a novel stiffness sensor which is mounted on the tip of a laparoscopic camera. The proposed device is able to compute stiffness when interacting with soft surfaces. The sensor can be used in Minimally Invasive Surgery, for instance, to localise tumor tissue which commonly has a higher stiffness when compared to healthy tissue. The purely mechanical sensor structure utilizes the functionality of an endoscopic camera to the maximum by visually analysing the behaviour of trackers within the field of view. Two pairs of spheres (used as easily identifiable features in the camera images) are connected to two springs with known but different spring constants. Four individual indenters attached to the spheres are used to palpate the surface. During palpation, the spheres move linearly towards the objective lens (i.e. the distance between lens and spheres is changing) resulting in variations of their diameters in the camera images. Relating the measured diameters to the different spring constants, a developed mathematical model is able to determine the surface stiffness in real-time. Tests were performed using a surgical endoscope to palpate silicon phantoms presenting different stiffness. Results show that the accuracy of the sensing system developed increases with the softness of the examined tissue.**

I. Introduction

Minimally Invasive Surgery (MIS) also know as key-hole or laparoscopic surgery has revolutionised the surgical care significantly reducing postoperative pain, recovery time and hospital stays with marked improvements in cosmetic outcome and overall cost-effectiveness [1]. Since the early 1990s, surgeons have been pushing the limit of MIS by attempting the most complicated procedures known in surgery. Minimally invasive techniques are now being utilized not only in relatively simpler operations such as prostatectomy [2], and cholecystectomy [3] but also in challenging practices which are very difficult to conduct laparoscopically such as coronary artery revascularization and mitral valve repair [5]. MIS involves procedures performed by entering the human body using instruments that are inserted via 12-15 mm incisions called Trocar ports. However, it is reported that the absence of physical tissue interaction is a major limitation of MIS compared to traditional open surgeries [6]. During open procedures, surgeons have direct access to affected organs. Surgeons investigate manually the force-displacement response to acquire distributed tactile information. Tissue areas that are stiffer than the surrounding tissue can be recognised as potentially abnormal and tumourous [7]. In MIS, surgeons rely on visual feedback of 2D or 3D endoscopic cameras [8]. An endoscope is a medical device consisting of a long, thin, flexible or rigid tube with an integrated camera and a light source at the tip. Images of the inside the patient's body can be displayed on a screen in real-time [9]. Endoscopes are mainly used for medical diagnosis and therapy to examine difficult-to-access areas and body regions to facilitate diagnosis of hidden diseases. Today, these instruments play an important role in medicine [10]. Performing safe surgeries in limited space and dynamic environments where surgeons have a restricted view and no sense of touch have created a growing demand on surgical vision techniques and sensor developments in order to retrieve tactile feedback. Analysis show that a new design is required to address these problems that occur with the current equipment [6]. Tactile and force sensors have been applied to surgical tools in MIS to measure local tissue properties [11] [12] [13]. Providing this feedback supports the surgeon operating with remote mechanisms. Many researchers use commercially available force sensors such as the ATI Nano17 (ATI, Industrial Automation), to measure force and torque accurately [14] [15]. However, constraints on size, geometry, costs, bio-compatibility and

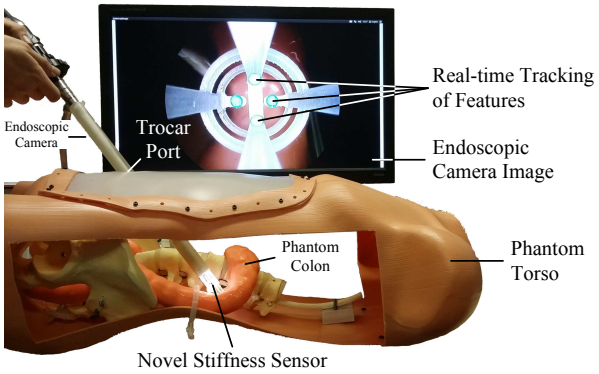

Fig. 1: Novel vision-based stiffness sensor mounted on an endoscopic camera inside a human phantom torso.

*The work described in this paper is partially funded by the Seventh Framework Programme of the European Commission under grant agreement 287728 in the framework of EU project STIFF-FLOP, as well as by the National Institute for Health Research (NIHR) Biomedical Research Centre based at Guy's and St Thomas' NHS Foundation Trust and King's College London. The views expressed are those of the authors and not necessarily those of the NHS, the NIHR or the Department of Health.

A. Faragasso, A. Stilli, J. Bimbo, Y. Noh, H. Liu, T. Nanayakkara, H.A. Wurdemann and K. Althoefer are with the Centre for Robotics Research, King's College London, London, UK. angela.faragasso, agostino.stilli, joao.bimbo, yohan.noh, hongbin.liu, thrish.antha, helge.wurdemann, k.althoefer@kcl.ac.uk

P. Dasgupta is with the Department of Urology, Guy's and St Thomas' Hospitals, NHS Foundation Trust, Guys Hospital, King's College London, UK. rokarurol@gmail.com

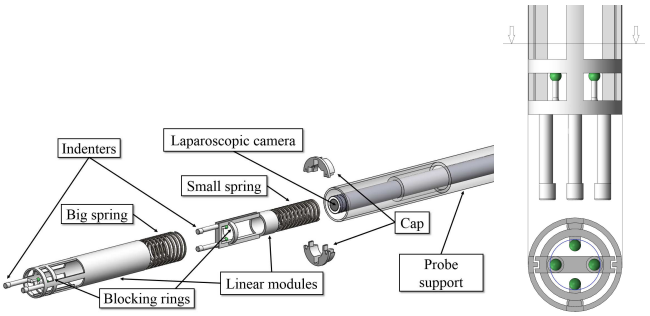

Fig. 2: CAD Drawing of the Vision based Stiffness sensor. (a) Exploited and (b) Section view showing the camera Field of View (FOV).

sterelisability make some of these approaches not suitable for MIS. A micro-electro mechanical system (MEMS) for stiffness measurement by employing sensing element with different stiffness was designed in [16], for instance.

In an earlier paper, we proposed a sensor device also based on spheres connected to springs moving in front of a camera, allowing us to measure force [17]. A sperical sphere is mounted on a endoscopic USB camera using a spring mechanism. Forces exerted to the sphere result in linear movements towards the camera. Hence, the spherical feature diameter varies in the camera image. A mathematical model determines the forces considering the known spring constant. Due to the size of the vision-based sensor, this device is not suitable for MIS. In addition, it uses a commercial available endoscopic USB camera which is not sterilizable. Most importantly, it can only measure force, while our sensing system proposed here is capable of measuring stiffness.
We propose a new vision-based stiffness sensor as shown in Figure 1. The sensorised probe is designed to be mounted on a laparoscopic camera. Our method soly relies on feature detection of a spring mechanism in provided the image data by the endoscopic camera. The advantages of our system are:

1) The sensing system computes stiffness based on vision data by an endoscopic camera. Since these cameras are usually deployed in laparoscopic surgery, their functionality is enhanced using the provided data for stiffness measurements too.
2) Our device has a simple mechanical miniaturiseable structure. Hence, the MR-compatible prototype described in this paper for endoscopic cameras will be able to meet the size limitations for MIS.
3) The sensing range and resolution can easily be modified by adjusting the two springs embedded inside the mechanism. Springs with a lower spring constant enable high force resolution sacrificing range and *vice-versa*.
4) The sensor's accuracy increases with the softness of the tissue. This feature makes the system high suitable for medical application.

II. Vision-based Force-Stiffness Sensor Design

The assembled prototype of the designed probe mounted on the laparoscopic camera is inserted into a human phantom torso in Figure 1. Here, we used a rigid endoscope, ENDOCAM® Performance HD by Richard Wolf GmbH (30 fps at 60 Hz), but the sensor can be designed for any surgical camera. An exploded view of the probe's drawing is shown in Figure 2(a). The prototype has been manufactured with a rapid prototyping machine (Project HD-3000 Plus, 3D Systems). The sensory device consists of a support structure, two linear modules connected to two spheres, a cap and two steel springs (see Figure 2(b)). The small spring has an outer diameter of $12.19\,\mathrm{mm}$, a wire diameter of $0.51\,\mathrm{mm}$ and an elastic constant of $40\,\frac{\mathrm{N}}{\mathrm{m}}$; the big one has an outer diameter of $16.76\,\mathrm{mm}$, a wire diameter of $0.74\,\mathrm{mm}$ and an elastic constant of $190\,\frac{\mathrm{N}}{\mathrm{m}}$. Both springs are made of SS316 steel which is MR-compatible. These springs are commercially available springs by Lee Spring Company. The springs are placed inside a hollow cylindrical support structure which is mounted on the laparoscope. Two linear modules with diameters equivalent to the sizes of the two springs are placed onto the end of the springs. Hence, the indenters at the tip of the linear modules with two spheres with a diameter of $2\,\mathrm{mm}$ are able to move independently. A cap fixes the linear guide and the springs inside the support structure. If equal forces are applied to the sensor tip, the four spheres will be an equal distance away from the camera lens. Two spheres are chosen for each linear module, so that a symmetrical arrangement is achieved with each having the same offset to the centre of the image plane as shown in Figure 2(b). The maximum indentation depth is $18\,\mathrm{mm}$ for this prototype. The diameter of the camera embedded with the sensory system is $19.5\,\mathrm{mm}$.

III. Visual Processing Algorithm

For image processing, we use the open source computer vision system OpenCV in ROS (Robot Operating System). The camera is calibrated and any lens distortion of the images is compensated. A customized image processing algorithm is implemented. This is based on the detection and tracking of a coloured sphere in the HSV color channel. A script allows to determine the colour interval online

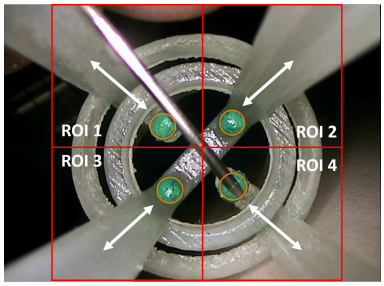

Fig. 3: 4 Regions of Interest (ROIs). The white arrows represent the possible direction of movement of each detected sphere (orange). In ROI 1, light reflection occurred and the sphere is partially occluded. ROI 4 shows that the algorithm can detect the sphere even in the case of 50% of occlusion.

and adapting the algorithm in case of any change in the illumination of the environment or the colour of the features. The tracking algorithm applies the morphological operator in a black/white image to select equivalent pixels in the HSV interval. Thus, it is possible to define the properties of areas in the image. Inner fragmentary regions are filled and bays along the corners are eliminated applying a sequence of two morphological primitives: dilate and erode. Noise and false positives are removed using the Gaussian blur filter. Hence, the implemented algorithm successfully detects the minimum enclosing circle containing all white points in the black/white image. In order to minimise errors in the computation of the radii, the image is subdivided into four Region of Interests (ROIs). In each of the ROIs, tracking of the spheres is performed as shown in Figure 3. The algorithm is robust to occlusions as well as to small reflections due to disturbing lightening (called specularity). This is demonstrated in ROI 4 of Figure 3, where the orange circle shows the successful detection of the sphere. Here, the spherical feature in ROI 1 is even detected if specularity occurs. This algorithm allows accurately computing the radius of the spherical features which will be used to characterise stiffness properties of phantom tissue.

IV. Modelling Force and Stiffness

A. Mathematical Model

The pinhole camera model defines the mathematical relationship between 3D point coordinates and their projection onto an image plane of an ideal pinhole camera. This ideal model can be used for a first order approximation of mapping a 3D scene to a 2D image. This transformation is called a perspective projection. We considered the relation between the sphere's radius into the 2D image when the two linear modules are indented during palpation. As the feature has a spherical shape and the embedded sensor allows movements only along a single axis that is perpendicular to the camera, the variation of the sphere's radius in the image can be related to its distance to the camera lens. We defined x as the distance between the camera centre and the projection of the sphere's position on the optical axis, h as the distance between the sphere and the optical axis and p as the line between the sphere's centre and its projection in the image plane that passes through the camera centre. It is possible to express Δx in function of h and p which yields:

$$\Delta x = x_0 - x_1 = x_0 - \sqrt{p_1^2 - h^2} \tag{1}$$

The values of x_0 and h are known. From the sensor's geometry the expression of p_1 is a function of the radius [17].

$$p_1 = \frac{r_0}{r} p_0 \tag{2}$$

In order to obtain the force,assuming a linear behaviour, Hooke's law is inserted into Equation 1, so that:

$$F(r) = K\Delta x(r) = K\left(x_0 - \sqrt{\frac{r_0^2}{r^2}p_0^2 - h^2}\right) \tag{3}$$

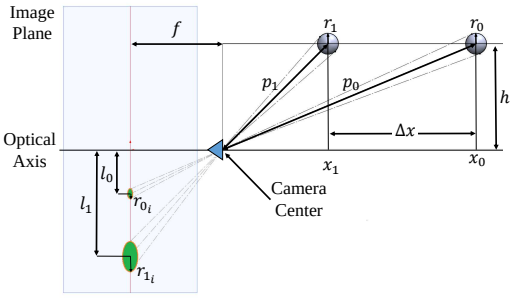

Fig. 4: Operating optical principle.The projection of the radius r_0 in the image plane r_{0i} is smaller than the projection of the radius r_1 being associates to a smaller camera-sphere distance. The focal length f is the distance between the camera centre and the image plane.

Here, K represents the spring constant. The returned force value depends on the design of the sensor and the size of the visual feature, i.e. the initial radius r_0 and projection of the feature-camera distance x_0 on the optical axis. In addition, the sphere's radius can be substituted with other geometrical parameters making its validation independent of the visual features shape. As explained in Section II, two features are each connected to a linear module with different spring constants. During contact with the surface of soft tissue, the linear module with a lower elastic constant is displaced more than the module with a higher elastic constant as shown in Figure 5. Since the indenters deform the tissue surface close to each other, interferences occur with regards to the indentation depth which will be neglected here as shown in Figure 5:

$$F_1 = K_1\Delta x_1 = Ks\Delta s_1 = F_{s1} \tag{4}$$

$$F_2 = K_2\Delta x_2 = Ks\Delta s_2 = F_{s2} \tag{5}$$

From Equations 4 and 5, the stiffness of the surface K_s is derived as:

$$K_s = \frac{F_1 - F_2}{\Delta s_1 - \Delta s_2} = \frac{(K_1\Delta x_1 - K_2\Delta x_2)}{\Delta d} \tag{6}$$

Applying force F_1 and F_2 the soft surface will deforms of d_1 and d_2 respectively. These two values will define a line in the F - Δd space. The slope of this line represents K_s.

V. Experimental Results

Experimental tests were performed using a laparoscopic camera to palpate silicon phantoms with different stiffness.

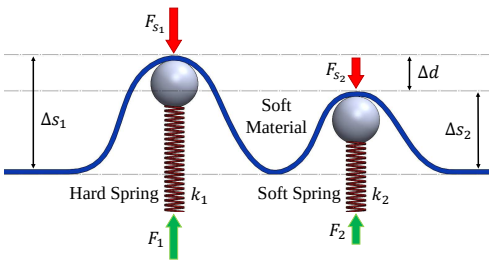

Fig. 5: Operating mechanical principle. Contact between the soft surface and the sensor showing the interacting forces and the differential force.

The silicon was placed on the top of a ATI Nano 17 F/T sensor which was used as ground truth and moved towards the sensing device using a linear guide. Endoscopic images were processed in real time. The force obtained from the benchmarking sensor is the sum of the two forces computed with our model [17]. The difference between the projection of the spheres' radius and the camera centre used to compute Δd increases with the softness of the tissue as a result of considerable displacement between the coupled features. A rigid body exhibits infinite stiffness which results in $\Delta d = 0$ in our model due to a null displacement between the coupled features. In this case, the stiffness is undefined as reported in Table I. Stress tests were performed to derive the stiffness of four silicon phantoms. This was compared with to the stiffness calculated by Equation 5. Figure 6 shows the linear trends Δx for the soft spring (Δx_1) and the stiffer (Δx_2) during a forward (indentation) and backward movement of the linear guide. The displacement Δx increases with time in the forward motion because of the elasticity difference of the springs, and *viceversa*. Table I reports accuracy analysis of our model. The accuracy decrease with the increasing of the tissue stiffness.

TABLE I: Accuracy Evaluation

Stiffness material (N/m)	Computed Stiffness (N/m)	Accuracy
0.0856	0.0859	99%
0.6423	0.6166	96%
1.8946	1.8367	96%
2.2373	2.1424	95%
∞	undefined	100%

VI. Discussion and Conclusions

In this paper, a novel stiffness sensor mechanism has been proposed which utilises visual information to compute the stiffness of soft tissue tracking linear elastic movements of visual features. Our sensor was developed for a laparoscopic camera; however, the sensing principle can be used for different purposes, such as object manipulations, autonomous navigation, human-robot collaboration. Here, we explained our approach for design and the implementation of a new sensing system, which to the best of authors's knowledge is the first implementation of a stiffness sensing device that only relies to visual information. The experimental results show that the mathematical model derived can compute the stiffness of soft tissue with high accuracy. The limitation and the inaccuracies of the sensor are mostly due to the friction and the parallel mechanism of the springs that will be addressed in future work. Further development of this sensing device will also consider the obstructions on the camera field of view and studies on the interference between the indenters.

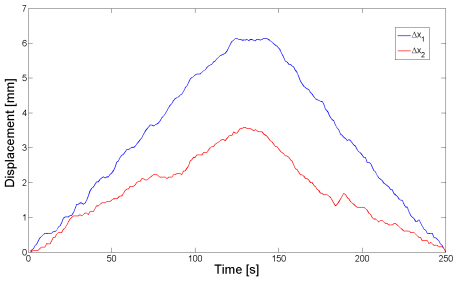

Fig. 6: The pattern of (Δx_1) and (Δx_2) displacements. In forward and backward motion.

References

[1] S. A. Darzi and Y. Munz, "The impact of minimally invasive surgical techniques," *Annual review of medicine*, vol. 55, pp. 223–37, Jan. 2004.

[2] J. C. Hu, Q. Wang, C. L. Pashos, S. R. Lipsitz, and N. L. Keating, "Utilization and outcomes of minimally invasive radical prostatectomy," *Journal of clinical oncology : official journal of the American Society of Clinical Oncology*, vol. 26, pp. 2278–84, May 2008.

[3] R. Hoffmann, "[Laparoscopic laser cholecystectomy]," *Therapeutische Umschau. Revue thérapeutique*, vol. 50, pp. 582–7, Aug. 1993.

[4] M. E. Currie, J. Romsa, S. Fox, W. Vezina, C. Akincioglu, J. Warrington, R. McClure, L. Stit, A. Menkis, W. Boyd, and B. Kiaii, "Long-term angiographic follow-up of robotic-assisted coronary artery revascularization," *The Annals of Thoracic Surgery*, vol. 93 (5), p. 142631, 2012.

[5] L. H. Cohn, D. H. Adams, G. S. Couper, D. P. Bichell, D. M. Rosborough, S. P. Sears, and S. F. Aranki, "Minimally invasive cardiac valve surgery improves patient satisfaction while reducing costs of cardiac valve replacement and repair," *Annals of surgery*, vol. 226, pp. 421–6; discussion 427–8, Oct. 1997.

[6] M. van Veelen, E. Nederlof, R. Goossens, C. Schot, and J. Jakimowicz, "Ergonomic problems encountered by the medical team related to products used for minimally invasive surgery," *Surg Endosc*, vol. 17, no. 7, pp. 1077–81, 2003.

[7] H. Stassen, J. Dankelman, and C. Grimbergen, "Developments in Minimally Invasive Surgery and Interventional Techniques (MISIT)," *Conference on human decision making and manual control*, pp. 212–218, 1997.

[8] P. Valdastri, M. Simi, and R. J. Webster, "Advanced technologies for gastrointestinal endoscopy," *Annual review of biomedical engineering*, vol. 14, pp. 397–429, Jan. 2012.

[9] J. Mitchell, "Endoscopy," *Annal of the Royal College of Surgeon of England*, vol. 62, pp. 106–111, 19780.

[10] N. Tanigawa, "Advantages and Problems with Endoscopic," vol. 137, no. 9, pp. 1833–1837, 2009.

[11] H. Liu, D. P. Noonan, B. J. Challacombe, P. Dasgupta, L. D. Seneviratne, and K. Althoefer, "Rolling mechanical imaging for tissue abnormality localization during minimally invasive surgery," *IEEE transactions on bio-medical engineering*, vol. 57, pp. 404–14, Feb. 2010.

[12] P. Polygerinos, A. Ataollahi, T. Schaeffter, R. Razavi, L. D. Seneviratne, and K. Althoefer, "MRI-compatible intensity-modulated force sensor for cardiac catheterization procedures.," *IEEE transactions on bio-medical engineering*, vol. 58, pp. 721–6, Mar. 2011.

[13] J. Rosen, B. Hannaford, M. P. MacFarlane, and M. N. Sinanan, "Force controlled and teleoperated endoscopic grasper for minimally invasive surgery–experimental performance evaluation," *IEEE transactions on bio-medical engineering*, vol. 46, pp. 1212–21, Oct. 1999.

[14] P. Puangmali, H. Liu, L. D. Seneviratne, P. Dasgupta, and K. Althoefer, "Miniature 3-axis distal force sensor for minimally invasive surgical palpation," *IEEEASME Transactions on Mechatronics*, vol. 17, no. 4, pp. 1–11, 2011.

[15] T. Yamamoto, B. Vgvlgyi, K. Balaji, L. L. Whitcomb, and A. M. Okamura, "Tissue property estimation and graphical display for teleoperated robot-assisted surgery.," in *ICRA*, pp. 4239–4245, IEEE, 2009.

[16] P. Peng, a. S. Sezen, R. Rajamani, and a. G. Erdman, "Novel MEMS stiffness sensor for in-vivo tissue characterization measurement," *Conference proceedings : Annual International Conference of the IEEE Engineering in Medicine and Biology Society. IEEE Engineering in Medicine and Biology Society. Conference*, vol. 2009, pp. 6640–3, Jan. 2009.

[17] A. Faragasso, J. Bimbo, Y. Noh, H. A. Wurdemann, S. Sareh, H. Liu, T. Nanayakkara, and K. Althoefer, "Novel Uniaxial Force Sensor based on Visual Information for Minimally Invasive Surgery," *IEEE International Conference on Robotics and Automation (ICRA)*, 2014.